


The dominant dependence of  $\Delta\alpha(t)$  expected from theory is logarithmic. However within the kinematic region of this analysis it may be approximated with a straight line. There is no statistical sensitivity to deviations from a linear behaviour of the running. So we fitted the ratios as:

$$R(t) = a + b|t| \quad (7)$$

The  $b$  slope represents the full observable effect of the running of  $\alpha(t)$ , both the leptonic and the hadronic component. It is related to the variation of the coupling by:

$$b = 2 \frac{\Delta\alpha(t_2) - \Delta\alpha(t_1)}{|t_2| - |t_1|} = \frac{2}{|t_2| - |t_1|} \frac{\alpha^{-1}(t_2) - \alpha^{-1}(t_1)}{\alpha_0^{-1}} \quad (8)$$

where  $t_1$  and  $t_2$  correspond to the acceptance limits. 1

- The hadronic contribution to the vacuum polarization is included in the Monte Carlo with the parameterization [16] of the form :

$$\Delta\alpha_{had} = A + B \ln(1 + C|t|) \quad (9)$$

The coefficients A, B and C have different values in intervals of  $|t|$  which depend on the detailed method of extraction of the parameterization. We fixed A and C to their values at the average  $|t|$  of our data sample, leaving B as a free parameter. In this case the leptonic contribution to the vacuum polarization  $\Delta\alpha_{lep}$  was kept at the calculated value.

The effective slope defined in (7) is slightly variable for the different data samples, as their average centre-of-mass energy varies. To combine the results we can practically redefine  $b$  in (7) as:

$$b = b^* \frac{\Delta t^*}{\Delta t} \quad (10)$$

where  $\Delta t$  is the actual energy-dependent  $t$  range,  $\Delta t^*$  corresponds to a reference centre-of-mass energy  $\sqrt{s} = 91.1$  GeV, and then fit for  $b^*$ . With the acceptance cuts specified in section 4 the reference  $t$  range is:  $t_1^* = -1.78$  GeV<sup>2</sup>,  $t_2^* = -5.96$  GeV<sup>2</sup>,  $\Delta t^* = |t_2^*| - |t_1^*| = 4.18$  GeV<sup>2</sup>.



### 3 Detector, data samples and Monte Carlo simulation

The OPAL detector and trigger have been described in detail elsewhere [17]. In particular this analysis is based on the silicon-tungsten luminometer (SiW), which was used to determine the luminosity from the counting rate of accepted Bhabha events, starting from 1993. The SiW was designed to improve the precision of the luminosity measurement to better than 1 per mille. In fact it achieved a fractional experimental systematic error of  $3.4 \times 10^{-4}$ . The detector and the luminosity measurement are extensively described in [12]. Here we only review briefly the detector aspects relevant for this analysis.

The OPAL SiW luminometer consisted of 2 identical cylindrical calorimeters, encircling the beam pipe symmetrically at about  $\pm 2.5$  m from the interaction point. Each calorimeter is a stack of 19 silicon layers interleaved with 18 tungsten plates, with a sensitive depth of 14 cm, representing 22 radiation lengths ( $X_0$ ). The first 14 tungsten plates are each 1  $X_0$  thick, while

# Summary of Comments on paper.1.0.dvi

---

## Page: 5

---

Sequence number: 1

Author: Richard Kellogg

Subject: Note

Date: 14.4.2004 2:54:16 PM

 after sent containing Eq. 8:

add:

The parameter  $a$  is not relevant, but is approximately 1, since the Monte Carlo is normalized to the data.


---

Sequence number: 2

Author: Richard Kellogg


Subject: Note

Date: 14.4.2004 2:36:03 PM

 end of sec 2:

give expected value of  $b$ . Discuss the scale of systematic effects which could mimic the expected running ala your email of 2-apr-2004

---

the last 4 are each  $2 X_0$  thick. The sensitive area fully covers radii between 6.2 and 14.2 cm from the beam axis. Each detector layer is segmented with  $R - \phi$  geometry in a  $32 \times 32$  pad array. The pad size is 2.5 mm radially and 11.25 degrees in azimuth. In total the whole luminometer had 38,912 readout channels corresponding to the individual silicon pads. The calibration was studied with electrical pulses generated both on the readout chips and on the front-end boards, as well as with ionization signals generated in the silicon using test beams and laboratory sources. Overall pad-to-pad gain variations were within 1%. 

We use the data samples collected in 1993-95 at energies close to the  $Z$  resonance peak. In total they amount to  $101 \text{ pb}^{-1}$  of OPAL data.

For the LEP2 data-taking started in 1996 the detector configuration changed, with the installation of tungsten shields designed to protect the inner tracking detectors from synchrotron radiation. These introduced about 50 radiation lengths of material in front of the calorimeters between 26 and 33 mrad from the beam axis, thus reducing the useful acceptance of the detector at the lower polar angle limit. Moreover the new fiducial acceptance cut fell right in the middle of the previous acceptance, where the preshowering material was maximum. For these reasons we have limited this analysis to the LEP1 data samples.

The OPAL SiW detector simulation does not rely on a detailed physical simulation of electromagnetic showers in the detector. Instead it is based on a parameterization of the detector response obtained from the data [12]. This approach gives a much more reliable description of the tails of the detector response functions, which are primarily due to extreme fluctuations in shower development, than we could obtain using any existing program which attempts to simulate the basic interactions of electrons and photons in matter. The measured LEP beam size and divergence, as well as the measured offset and tilt of the beam with respect to the calorimeters are also incorporated in this simulation. The Monte Carlo simulation is used to correct the acceptance for the effects of the detector energy response, the coordinate resolution and LEP beam parameters. The data are divided in 9 subsamples according to the average centre-of-mass energy and the values of the beam parameters, which slightly varied. For each subsample we generated an independent sample of BHLUMI events subjected to detector simulation with corresponding setting of the parameters. The statistics were always at least 10 times those of the corresponding data set.

There are other acceptance corrections which are not accounted by the Monte Carlo simulation, but rather applied directly to data. These include the trigger efficiency, accidental background, detector metrology and most importantly biases in the reconstructed radial coordinate. The latter is crucial for this analysis and will be discussed in section 5.

## 4 Event selection

The event selection criteria can be classified into *isolation* cuts, which isolate a sample of pure Bhabha scattering events from the off-momentum background, and acceptance defining, or *definition* cuts. The isolation cuts are used to define a fiducial set of events which lie within the good acceptance of both calorimeters and are essentially background free. The definition cuts then select subsets of events from within the fiducial sample. Showers generated by incident electrons and photons are recognized as clusters in the calorimeters and their energies and

# Page: 6


---

Sequence number: 1

Author: Richard Kellogg

Subject: Note

Date: 14.4.2004 3:03:48 PM

 after sec 3 par 2:

add plot of pre-showering material (pr289\_03.eps) & discuss.

---

to the true  $\sigma$ . The uncertainty on the conversion factor from  $\sigma_a$  to  $\sigma$  has been estimated from the difference between the test beam with no additional material and with  $0.84 X_0$  of material in front of the detector.

In OPAL data  $R_{off}$  measures the shift of the observed pad boundary image from the nominal position of the pad boundary. Such shifts can be produced by a large number of causes: pad gain fluctuations, metrology shifts, detector malfunctions, resolution effects and preshowering. The pad boundary bias is determined by converting the apparent  $\sigma_a$  to the true  $\sigma$  and then using the test beam results to find the corresponding geometric bias. Fig. 2 shows that a gaussian resolution does not perfectly describe the tails of the distribution. To the extent that the pad boundary image maintains an odd symmetry about the apparent pad boundary, its non-gaussian behaviour does not affect the determination of  $R_{off}$  as can be seen from the close agreement of the data points and the fitted curve near the pad boundary. We have also considered a model in which the apparent pad boundary is taken as the **1 median of the observed resolution function**. The difference between the two models is assigned as a systematic error of the fit method, when it is larger than the fit statistical error, otherwise the latter is kept as estimate. **2 further difference of the test beam with respect to the OPAL data is that it was carried out at a radial position close to the inner acceptance cut**. The geometrical bias due to  $R - \phi$  pads is expected to scale as  $1/R$ , thus decreasing at a greater radius of pad curvature. Therefore we have scaled in this way the bias estimated by using the test beam results, but assign an additional systematic error equal to 50% of the expected bias to account for possible deviations from this behaviour.

The total net bias (also called *anchor*)  $\delta R$  on the position of a pad boundary is given by:

$$\delta R = R_{off} + \delta R_{R\phi} + \delta R_{res} \quad (11)$$

where  $R_{off}$  is the coordinate offset which may have positive or negative sign,  $\delta R_{R\phi}$  is the pad boundary bias, always positive and  $\delta R_{res}$  is a small (positive) additional bias due to the **3 resolution flow**. The latter results from the steeply falling radial resolution and can be thought as a second-order effect.

From Fig. 2 one can see that the width is similar at the inner and outer radius, while it is considerably greater at the central radius. The offset  **$R_{off}$  is found very small** at the inner edge while it increases to  $\approx 10 - 20 \mu\text{m}$  at the central and the outer radius. Among other effects, the observed  $R_{off}$  is affected by **fluctuations in the pad gain**. We have checked these effects directly on data, by studying  $R_{off}$  as a function of the 32 azimuthal divisions of the calorimeters. We assign the size of the azimuthal variations,  $(R_{off})_{RMS}/\sqrt{32}$ , as a systematic error in the anchors, due to pad gain variations.

The anchors determined from 1993-94 data for the layers at  **$4 X_0$  and all the pad boundaries** used in the analysis are shown in Fig. 3. A similar trend is **visible in the two sides**, in particular the rise of the anchor from about zero at the inner edge to  $20 - 25 \mu\text{m}$  around  $R = 9 \text{ cm}$ . The inner error bars are the statistical errors in the fit of the pad boundary images. The full error bars include in quadrature the systematic errors **from: fit method, pad gain variations,  $\sigma_a$  conversion, test beam parameterization and the assumed  $1/R$  scaling of the pad boundary bias**. The anchors determined from 1995 data have similar features although with lower statistics.

The anchors have been determined separately for 1993-94 and 1995 data, because the amount of preshowering material was different in the two sub-samples. A clear relation with the amount

## Page: 9

---

Sequence number: 1  
Author: Richard Kellogg  
Subject: Highlight  
Date: 13.4.2004 3:57:59 PM

**T** median of the observed resolution function

question:

Do you mean "mean" rather than "median" here? I believe the method already described finds the median.

---

Sequence number: 2  
Author: Richard Kellogg  
Subject: Highlight  
Date: 14.4.2004 6:39:39 PM

**T** replace:

A further difference of the test beam with respect to the OPAL data is that it was carried out at a radial position close to the inner acceptance cut

with:

The determination of the pad boundary bias in the test beam was carried out at a radial position close to the inner acceptance cut to provide optimal information for the luminosity determination. In this analysis we have a greater dependence on knowing the pad boundary bias throughout the detector.

---

Sequence number: 3  
Author: Richard Kellogg  
Subject: Highlight  
Date: 13.4.2004 4:30:20 PM

**T** replace:

resolution flow. The latter results from the steeply falling radial resolution and can be thought as a second-order effect.

with:

{\em resolution flow}. This second order effect arises whenever a cut is imposed on a quantity with a steeply falling distribution. An acceptance change is introduced due to the fact that more events actually on the uphill side of the cut will be measured to fall on the downhill side than vice--versa. This resolution flow can be expressed as

$$\begin{equation} \frac{\Delta A}{A} = \frac{\langle d \rangle}{\langle d \rangle x} \frac{\sigma_x^2}{2} \end{equation} \label{eq:resflow}$$

\noindent

where  $f(x)$  is the intensity of events normalized to unity over the entire acceptance, and  $\sigma_x$  is the resolution in the variable  $x$  upon

Comments from page 9 continued on next page

to the true  $\sigma$ . The uncertainty on the conversion factor from  $\sigma_a$  to  $\sigma$  has been estimated from the difference between the test beam with no additional material and with  $0.84 X_0$  of material in front of the detector.

In OPAL data  $R_{off}$  measures the shift of the observed pad boundary image from the nominal position of the pad boundary. Such shifts can be produced by a large number of causes: pad gain fluctuations, metrology shifts, detector malfunctions, resolution effects and preshowering. The pad boundary bias is determined by converting the apparent  $\sigma_a$  to the true  $\sigma$  and then using the test beam results to find the corresponding geometric bias. Fig. 2 shows that a gaussian resolution does not perfectly describe the tails of the distribution. To the extent that the pad boundary image maintains an odd symmetry about the apparent pad boundary, its non-gaussian behaviour does not affect the determination of  $R_{off}$  as can be seen from the close agreement of the data points and the fitted curve near the pad boundary. We have also considered a model in which the apparent pad boundary is taken as the **median of the observed resolution function**. The difference between the two models is assigned as a systematic error of the fit method, when it is larger than the fit statistical error, otherwise the latter is kept as estimate. **A further difference of the test beam with respect to the OPAL data is that it was carried out at a radial position close to the inner acceptance cut.** The geometrical bias due to  $R - \phi$  pads is expected to scale as  $1/R$ , thus decreasing at a greater radius of pad curvature. Therefore we have scaled in this way the bias estimated by using the test beam results, but assign an additional systematic error equal to 50% of the expected bias to account for possible deviations from this behaviour.

The total net bias (also called *anchor*)  $\delta R$  on the position of a pad boundary is given by:

$$\delta R = R_{off} + \delta R_{R\phi} + \delta R_{res} \quad (11)$$

where  $R_{off}$  is the coordinate offset which may have positive or negative sign,  $\delta R_{R\phi}$  is the pad boundary bias, always positive and  $\delta R_{res}$  is a small (positive) additional bias due to the **resolution flow. The latter results from the steeply falling radial resolution and can be thought as a second-order effect.**

From Fig. 2 one can see that the width is similar at the inner and outer radius, while it is considerably greater at the central radius. The offset **4<sub>off</sub> is found very small** at the inner edge while it increases to  $\approx 10 - 20 \mu\text{m}$  at the central and the outer radius. Among other effects, the observed  $R_{off}$  is affected by **5<sub>uctuations in the pad gain</sub>**. We have checked these effects directly on data, by studying  $R_{off}$  as a function of the 32 azimuthal divisions of the calorimeters. We assign the size of the azimuthal variations,  $(R_{off})_{RMS}/\sqrt{32}$ , as a systematic error in the anchors, due to pad gain vaiations.

The anchors determined from 1993-94 data for the layers at **6<sub>X0</sub> and all the pad boundaries** used in the analysis are shown in Fig. 3. A similar trend is **7<sub>sible in the two sides</sub>**, in particular the rise of the anchor from about zero at the inner edge to  $20 - 25 \mu\text{m}$  around  $R = 9 \text{ cm}$ . The inner error bars are the statistical errors in the fit of the pad boundary images. The full error bars include in quadrature the systematic errors **8<sub>om: fit method, pad gain variations,  $\sigma_a$  conversion, test beam parameterization and the assumed  $1/R$  scaling of the pad boundary bias.</sub>** The anchors determined from 1995 data have similar features although with lower statistics.

The anchors have been determined separately for 1993-94 and 1995 data, because the amount of preshowering material was different in the two sub-samples. A clear relation with the amount

which the cut is imposed.

---

Sequence number: 4  
Author: Richard Kellogg  
Subject: Highlight  
Date: 13.4.2004 4:30:59 PM

**T** replace:  
Roff is found very small

with:  
Roff is found to be very small

---

Sequence number: 5  
Author: Richard Kellogg  
Subject: Highlight  
Date: 14.4.2004 3:10:03 PM

**T** replace:  
fluctuations in the pad gain

with:  
fluctuations in the individual pad gains

---

Sequence number: 6  
Author: Richard Kellogg  
Subject: Highlight  
Date: 14.4.2004 3:10:48 PM

**T** replace:  
4 X0 and all the pad boundaries

with:  
4 X0 for all the pad

---

Sequence number: 7  
Author: Richard Kellogg  
Subject: Highlight  
Date: 14.4.2004 3:11:38 PM

**T** replace:  
visible in the two sides,

with;  
visible on the two sides,

---

Sequence number: 8  
Author: Richard Kellogg  
Subject: Highlight  
Date: 14.4.2004 3:14:48 PM

**T** replace:  
from: fit method, pad gain variations, sigma\_a conversion, test beam parameterization and the assumed 1/R scaling of the pad boundary bias.

with:  
from the fit method, pad gain variations, test beam parameterization and the assumed 1/R scaling and shower width dependence of the pad boundary bias.

---



and distribution of the material upstream of the calorimeters is visible from the apparent width  $\sigma_a$  as a function of radius, as shown in Fig. 4. The distribution of material upstream of the calorimeters was kept at a minimum especially in the crucial region of the inner acceptance cut where it amounts to  $0.25 X_0$ . In the middle of the acceptance this material increases to about  $2 X_0$  due to cables and support structures of the beam pipe. **1**he remarkable difference between the Right and Left widths in 1993-94 data is due to **2**assage of cables from the OPAL microvertex detector. For 1995 data additional cables were installed in the Right side, which restored an almost symmetrical situation. The presence of a non-negligible amount of preshowering material in the middle of the acceptance constitutes the most delicate **3**xperimental problem, as the anchoring procedure was developed and checked at the test beam only for the almost ideal situation of a bare calorimeter or of less than  $1 X_0$  of preshowering material. Therefore we checked thoroughly the anchoring procedure in OPAL data before trusting its results.

The acceptance of an individual radial bin with boundaries  $(R_{inn}, R_{out})$  is corrected by introducing the anchors  $\delta R_{inn}, \delta R_{out}$  determined as in (11) in the following formula, giving the fractional correction:

$$\frac{\delta A}{A} = c_{inn} \delta R_{inn} - c_{out} \delta R_{out} \quad (12)$$

The coefficients  $c_{inn}$  and  $c_{out}$  are derived by a simple analytical calculation assuming a  $1/\theta^3$  spectrum for the angular distribution and are given by:

$$c_k = \frac{\frac{1}{R_k^3}}{\frac{1}{2} \left( \frac{1}{R_{inn}^2} - \frac{1}{R_{out}^2} \right)} \quad k = \text{4}^{in, out} \quad (13)$$

The corrections are at most 0.5% (1%) for the Right (Left) side in 1993-94 data and 0.8% (0.7%) for the Right (Left) side in 1995 data.

The reconstructed radial coordinate can be studied by **5**multaneously varying the value of the radial cut in the data and in the Monte Carlo. The Monte Carlo assumes that the radial coordinate is reconstructed without bias. Thus any difference in the acceptance of the data and Monte Carlo as the inner cut is varied, beyond that expected from the finite statistics, can be attributed to biases in the radial coordinate. The relative acceptance, as a function of the value of **the inner radial definition cut is shown** for the Right and the Left side selection in Fig. 5 for 1993-94 data. The **width of the shaded bands** represents the binomial errors with respect to the reference selection  $7.20 \text{ cm} \leq R \leq 13.20 \text{ cm}$ . **The solid points show** the anchoring results for all the relevant pad boundaries in layers between  $1 X_0$  and  $10 X_0$ . **The estimated radial biases are converted into acceptance variations** using the formula:

$$\frac{\delta A}{A} = 2 \frac{R_{inn}^2 R_{out}^2}{R_{out}^2 - R_{inn}^2} \frac{\delta R}{R^3} \quad (14)$$

where  $R_{inn} = 7.20 \text{ cm}$ ,  $R_{out} = 13.20 \text{ cm}$  and  $R$  is varied from  $R_{inn}$  to  $R_{out}$ . Since the normalization is the total acceptance, the low  $R$  points have a greater weight in the plot, **as is implied by** the  $1/R^3$  dependence. Therefore any visible structure tends to be flattened at increasing radius.

**In the plot the anchor at the inner cut  $R = 7.20 \text{ cm}$  in layer  $7 X_0$  has been required to lie** at zero. Each group of nearby points, marked by either circles or triangles, refer to a given pad row boundary in different layers, that is at variable **depth into the calorimeters**. Since all the

# Page: 10

---

Sequence number: 1  
Author: Richard Kellogg  
Subject: Highlight  
Date: 13.4.2004 3:43:10 PM

**T**replace:  
The remarkable difference

with:  
The noticeable difference

---

Sequence number: 2  
Author: Richard Kellogg  
Subject: Highlight  
Date: 14.4.2004 3:15:55 PM

**T**replace:  
passage of cables  
with:  
presence of cables

---

Sequence number: 3  
Author: Richard Kellogg  
Subject: Highlight  
Date: 14.4.2004 4:41:57 PM

**T**replace:  
experimental problem, as the anchoring procedure was developed and checked at the test beam only for the almost ideal situation of a bare calorimeter or of less than 1 X0 of preshowering material.  
with:  
experimental problem for this analysis, since the anchoring procedure was developed and checked using the test beam only for the amount of preshowering material ( $< 1 X_0$ ) most relevant for the luminosity measurement.

---

Sequence number: 4  
Author: Richard Kellogg  
Subject: Highlight  
Date: 13.4.2004 3:45:37 PM

**T**replace(globally):  
inn

with:  
in

---

Sequence number: 5  
Author: Richard Kellogg  
Subject: Highlight  
Date: 14.4.2004 4:45:47 PM

**T**replace:

Comments from page 10 continued on next page

and distribution of the material upstream of the calorimeters is visible from the apparent width  $\sigma_a$  as a function of radius, as shown in Fig. 4. The distribution of material upstream of the calorimeters was kept at a minimum especially in the crucial region of the inner acceptance cut where it amounts to  $0.25 X_0$ . In the middle of the acceptance this material increases to about  $2 X_0$  due to cables and support structures of the beam pipe. The remarkable difference between the Right and Left widths in 1993-94 data is due to passage of cables from the OPAL microvertex detector. For 1995 data additional cables were installed in the Right side, which restored an almost symmetrical situation. The presence of a non-negligible amount of preshowering material in the middle of the acceptance constitutes the most delicate experimental problem, as the anchoring procedure was developed and checked at the test beam only for the almost ideal situation of a bare calorimeter or of less than  $1 X_0$  of preshowering material. Therefore we checked thoroughly the anchoring procedure in OPAL data before trusting its results.

The acceptance of an individual radial bin with boundaries  $(R_{inn}, R_{out})$  is corrected by introducing the anchors  $\delta R_{inn}, \delta R_{out}$  determined as in (11) in the following formula, giving the fractional correction:

$$\frac{\delta A}{A} = c_{inn} \delta R_{inn} - c_{out} \delta R_{out} \quad (12)$$

The coefficients  $c_{inn}$  and  $c_{out}$  are derived by a simple analytical calculation assuming a  $1/\theta^3$  spectrum for the angular distribution and are given by:

$$c_k = \frac{\frac{1}{R_k^3}}{\frac{1}{2} \left( \frac{1}{R_{inn}^2} - \frac{1}{R_{out}^2} \right)} \quad k = inn, out \quad (13)$$

The corrections are at most 0.5% (1%) for the Right (Left) side in 1993-94 data and 0.8% (0.7%) for the Right (Left) side in 1995 data.

The reconstructed radial coordinate can be studied by simultaneously varying the value of the radial cut in the data and in the Monte Carlo. The Monte Carlo assumes that the radial coordinate is reconstructed without bias. Thus any difference in the acceptance of the data and Monte Carlo as the inner cut is varied, beyond that expected from the finite statistics, can be attributed to biases in the radial coordinate. The relative acceptance, as a function of the value of the inner radial definition cut is shown for the Right and the Left side selection in Fig. 5 for 1993-94 data. The width of the shaded bands represents the binomial errors with respect to the reference selection  $7.20 \text{ cm} \leq R \leq 13.20 \text{ cm}$ . The solid points show the anchoring results for all the relevant pad boundaries in layers between  $1 X_0$  and  $10 X_0$ . The estimated radial biases are converted into acceptance variations using the formula:

$$\frac{\delta A}{A} = 2 \frac{R_{inn}^2 R_{out}^2}{R_{out}^2 - R_{inn}^2} \frac{\delta R}{R^3} \quad (14)$$

where  $R_{inn} = 7.20 \text{ cm}$ ,  $R_{out} = 13.20 \text{ cm}$  and  $R$  is varied from  $R_{inn}$  to  $R_{out}$ . Since the normalization is the total acceptance, the low  $R$  points have a greater weight in the plot, which is implied by the  $1/R^3$  dependence. Therefore any visible structure tends to be flattened at increasing radius.

In the plot the anchor at the inner cut  $R = 7.20 \text{ cm}$  in layer  $7 X_0$  has been required to lie at zero. Each group of nearby points, marked by either circles or triangles, refer to a given pad row boundary in different layers, that is at variable depth into the calorimeters. Since all the

simultaneously varying the value of the radial cut in the data and in the Monte Carlo.

with:

considering the ratio between the number of data events falling above a certain inner radius cut and the corresponding number of events in the Monte Carlo. We call this integral ratio the {relative acceptance}.

---

Sequence number: 6

Author: Richard Kellogg

Subject: Highlight

Date: 14.4.2004 4:48:29 PM

**T** replace:

the inner radial definition cut is shown

with:

the inner radial cut is shown as a shaded band

---

Sequence number: 7

Author: Richard Kellogg

Subject: Highlight

Date: 14.4.2004 4:49:31 PM

**T** replace:

width of the shaded bands

with:

width of the bands

---

Sequence number: 8

Author: Richard Kellogg

Subject: Highlight

Date: 14.4.2004 5:43:20 PM

**T** begin new paragraph with:

The solid points show

but at end of what will become the previous paragraph insert:

Note that, by construction, both ends of the relative acceptance band at  $R=7.2$  and  $R=13.2\text{cm}$  are required to lie at zero.

---

Sequence number: 9

Author: Richard Kellogg

Subject: Highlight

Date: 14.4.2004 4:51:31 PM

**T** replace:

The estimated radial biases are converted into acceptance variations

with:

The radial bias corresponding to each anchor is converted into an acceptance variation

---

Sequence number: 10

Author: Richard Kellogg

Subject: Highlight

Date: 14.4.2004 5:51:15 PM

**T** replace:

as is implied by

Comments from page 10 continued on next page

and distribution of the material upstream of the calorimeters is visible from the apparent width  $\sigma_a$  as a function of radius, as shown in Fig. 4. The distribution of material upstream of the calorimeters was kept at a minimum especially in the crucial region of the inner acceptance cut where it amounts to  $0.25 X_0$ . In the middle of the acceptance this material increases to about  $2 X_0$  due to cables and support structures of the beam pipe. The remarkable difference between the Right and Left widths in 1993-94 data is due to passage of cables from the OPAL microvertex detector. For 1995 data additional cables were installed in the Right side, which restored an almost symmetrical situation. The presence of a non-negligible amount of preshowering material in the middle of the acceptance constitutes the most delicate experimental problem, as the anchoring procedure was developed and checked at the test beam only for the almost ideal situation of a bare calorimeter or of less than  $1 X_0$  of preshowering material. Therefore we checked thoroughly the anchoring procedure in OPAL data before trusting its results.

The acceptance of an individual radial bin with boundaries  $(R_{inn}, R_{out})$  is corrected by introducing the anchors  $\delta R_{inn}, \delta R_{out}$  determined as in (11) in the following formula, giving the fractional correction:

$$\frac{\delta A}{A} = c_{inn} \delta R_{inn} - c_{out} \delta R_{out} \quad (12)$$

The coefficients  $c_{inn}$  and  $c_{out}$  are derived by a simple analytical calculation assuming a  $1/\theta^3$  spectrum for the angular distribution and are given by:

$$c_k = \frac{\frac{1}{R_k^3}}{\frac{1}{2} \left( \frac{1}{R_{inn}^2} - \frac{1}{R_{out}^2} \right)} \quad k = inn, out \quad (13)$$

The corrections are at most 0.5% (1%) for the Right (Left) side in 1993-94 data and 0.8% (0.7%) for the Right (Left) side in 1995 data.

The reconstructed radial coordinate can be studied by simultaneously varying the value of the radial cut in the data and in the Monte Carlo. The Monte Carlo assumes that the radial coordinate is reconstructed without bias. Thus any difference in the acceptance of the data and Monte Carlo as the inner cut is varied, beyond that expected from the finite statistics, can be attributed to biases in the radial coordinate. The relative acceptance, as a function of the value of the inner radial definition cut is shown for the Right and the Left side selection in Fig. 5 for 1993-94 data. The width of the shaded bands represents the binomial errors with respect to the reference selection  $7.20 \text{ cm} \leq R \leq 13.20 \text{ cm}$ . The solid points show the anchoring results for all the relevant pad boundaries in layers between  $1 X_0$  and  $10 X_0$ . The estimated radial biases are converted into acceptance variations using the formula:

$$\frac{\delta A}{A} = 2 \frac{R_{inn}^2 R_{out}^2}{R_{out}^2 - R_{inn}^2} \frac{\delta R}{R^3} \quad (14)$$

where  $R_{inn} = 7.20 \text{ cm}$ ,  $R_{out} = 13.20 \text{ cm}$  and  $R$  is varied from  $R_{inn}$  to  $R_{out}$ . Since the normalization is the total acceptance, the low  $R$  points have a greater weight in the plot, as is implied by the  $1/R^3$  dependence. Therefore any visible structure tends to be flattened at increasing radius.

11 the plot the anchor at the inner cut  $R = 7.20 \text{ cm}$  in layer  $7 X_0$  has been required to lie at zero. Each group of nearby points, marked by either circles or triangles, refer to a given pad row boundary in different layers, that is at variable 12 both into the calorimeters. Since all the

with:  
due to

---

Sequence number: 11  
Author: Richard Kellogg  
Subject: Highlight  
Date: 14.4.2004 5:55:55 PM

**T**replace:

In the plot the anchor at the inner cut  $R = 7.20$  cm in layer 7 X0 has been required to lie  
with:

Any of the anchors could be chosen to fix the absolute offset in the continuous radial coordinate, here we  
choose the anchor at  $R = 7.20$  cm in layer 7 X0 and this point correspondingly lies

---

Sequence number: 12  
Author: Richard Kellogg  
Subject: Highlight  
Date: 14.4.2004 5:57:32 PM

**T**replace:

depth into the calorimeters.

with:

depth in the calorimeters.

---

coordinates are projected to the **1**ference layer  $7 X_0$  they are spaced by about  $200 \mu\text{m}$  at the inner radius and by about  $350 \mu\text{m}$  at the outer radius **2**om one layer to the other. The arrows mark the position of a given pad row boundary in layer  $7 X_0$ , deeper layers have a lower  $R$  and shallower layers a higher  $R$ .

**3**s the plot shows the variation in the integrated acceptance, the most relevant thing to inspect is the slope of the acceptance variation as the radius is varied. Moreover the plot shows as reference the anchors in layer  $7 X_0$ , as the starting value at  $R = 7.20 \text{ cm}$  is set to zero, coincident with origin of the band. If an alternative layer is chosen the normalization should be done with respect to that point. The applicability of the method appears safe for the range of layers which give an almost flat behaviour, compatible with the shaded band. **4** discrepancy is apparent for the deepest layers considered ( $8 - 10 X_0$ ), in particular for the Left side. This is most evident in the central region of acceptance, where the amount of material between the detector and the interaction point is large and the test beam measurement of the expected bias may no longer be applicable. To stay away from such problems we have selected layer  $4 X_0$  as the central layer for anchoring, and checked the results with alternative anchors from layer  $1 X_0$  to layer  $7 X_0$ .

An amazing illustration of the anchoring capability is possible by downgrading the quality of the reconstructed radial coordinate and then determining the resulting (larger) radial biases. The last step in radial reconstruction before the anchoring procedure is a *smoothing* algorithm [12], which was implemented to remove a residual bias resulting from the variable position resolution across the pad structure of the detector. This bias has a maximum amplitude of  $\pm 50 \mu\text{m}$  and has a periodic structure with period equal to the  $2.5 \text{ mm}$  pad width. If we repeat the **game** of Fig. 5, switching off the smoothing from the radial reconstruction, the result is Fig. 6. The alternative anchors track the expected acceptance variations for each of the pad rows and most of the depth range studied. Similar considerations apply here as said before. The anchoring has been further checked in the following section 7.1.

## 6 Fit

The fit results on the nine data sets are shown in Table 1. Each number is obtained by a linear fit as (7) on 24 points. Data have been corrected with anchors on layer  $4 X_0$  and only the data statistical errors are considered. The nine samples give consistent results, with  $\chi^2$  of the average of  $6.5/8$  for the Right side and  $5.6/8$  for the Left side. However the quality of some of the individual fits is not good in particular on the Left side. Considering for example the largest dataset (94 b) the  $\chi^2$  of the linear fit (7) is  $27.8/22$  on the Right side and  $101.9/22$  on the Left side. To sharpen the sensitivity to correlated systematic effects we combined the six 1993-94 distributions, the three 1995 distributions and also all the nine distributions together. We checked the quality of the fits by including also the anchoring systematic errors, discussed in the previous section. They all have been conservatively considered uncorrelated as a function of radius, except for the error of the fit method. Uncorrelated errors on the anchors actually produce anti-correlations between adjacent bins. These short range effects may deteriorate greatly the fit  $\chi^2$  even if producing small effects on the fitted slope. We have then built  $24 \times 24$  covariance matrices implementing these systematic errors for radial distributions binned with 1 bin equal to 1 detector pad ( $2.5 \text{ mm}$ ). We checked the fit  $\chi^2$  both before and after the

# Page: 11

---

Sequence number: 1  
Author: Richard Kellogg  
Subject: Highlight  
Date: 14.4.2004 5:59:26 PM

**T**replace:  
reference layer 7 X0 they are spaced  
with:  
reference layer 7 X0 the pad boundaries at the same radius in adjacent layers are spaced

---

Sequence number: 2  
Author: Richard Kellogg  
Subject: Highlight  
Date: 14.4.2004 5:59:51 PM

**T**remove:  
from one layer to the other.

---

Sequence number: 3  
Author: Richard Kellogg  
Subject: Highlight  
Date: 14.4.2004 5:41:30 PM

**T**replace:  
As the plot shows the variation in the integrated acceptance, the most relevant thing to inspect is the slope of the acceptance variation as the radius is varied. Moreover the plot shows as reference the anchors in layer 7 X0, as the starting value at  $R = 7.20$  cm is set to zero, coincident with origin of the band. If an alternative layer is chosen the normalization should be done with respect to that point. The applicability of the method appears safe for the range of layers which give an almost flat behaviour, compatible with the shaded band  
with:  
The essential point of Fig. 5 is that the anchor points derived from individual pad boundaries should follow the relative acceptance band derived from the distribution of coordinates, since this shows that the two independent methods of determining shower positions in the calorimeter are in agreement. It must also be remembered that the choice of which anchor to use in fixing the global offset of the radial coordinate is arbitrary.

Almost all anchors are found to be consistent, even in those regions where the relative acceptance band reveals the presence of residual structure in the coordinate.

---

Sequence number: 4  
Author: Richard Kellogg  
Subject: Highlight  
Date: 14.4.2004 6:01:19 PM

**T**replace:  
A discrepancy is apparent  
with:  
Clear discrepancies are, however,

---



coordinates are projected to the reference layer  $7 X_0$  they are spaced by about  $200 \mu\text{m}$  at the inner radius and by about  $350 \mu\text{m}$  at the outer radius from one layer to the other. The arrows mark the position of a given pad row boundary in layer  $7 X_0$ , deeper layers have a lower  $R$  and shallower layers a higher  $R$ .

As the plot shows the variation in the integrated acceptance, the most relevant thing to inspect is the slope of the acceptance variation as the radius is varied. Moreover the plot shows as reference the anchors in layer  $7 X_0$ , as the starting value at  $R = 7.20 \text{ cm}$  is set to zero, coincident with origin of the band. If an alternative layer is chosen the normalization should be done with respect to that point. The applicability of the method appears safe for the range of layers which give an almost flat behaviour, compatible with the shaded band. A discrepancy is apparent for the deepest layers considered ( $8 - 10 X_0$ ), in particular for the Left side. This is most evident in the central region of acceptance, where the amount of material between the detector and the interaction point is large and the test beam measurement of the expected bias may no longer be applicable. To stay away from such problems we have selected layer  $4 X_0$  as the central layer for anchoring, and checked the results with alternative anchors from layer  $1 X_0$  to layer  $7 X_0$ .

An amazing illustration of the anchoring capability is possible by downgrading the quality of the reconstructed radial coordinate and then determining the resulting (larger) radial biases. The last step in radial reconstruction before the anchoring procedure is a *smoothing* algorithm [12], which was implemented to remove a residual bias resulting from the variable position resolution across the pad structure of the detector. This bias has a maximum amplitude of  $\pm 50 \mu\text{m}$  and has a periodic structure with period equal to the  $2.5 \text{ mm}$  pad width. If we repeat the same of Fig. 5, switching off the smoothing from the radial reconstruction, the result is Fig. 6. The alternative anchors track the expected acceptance variations for each of the pad rows and most of the depth range studied. Similar considerations apply here as said before. The anchoring has been further checked in the following section 7.1.

## 6 Fit

The fit results on the nine data sets are shown in Table 1. Each number is obtained by a linear fit as (7) on 24 points. Data have been corrected with anchors on layer  $4 X_0$  and only the data statistical errors are considered. The nine samples give consistent results, with  $\chi^2$  of the average of  $6.5/8$  for the Right side and  $5.6/8$  for the Left side. However the quality of some of the individual fits is not good in particular on the Left side. Considering for example the largest dataset (94 b) the  $\chi^2$  of the linear fit (7) is  $27.8/22$  on the Right side and  $101.9/22$  on the Left side. To sharpen the sensitivity to correlated systematic effects we combined the six 1993-94 distributions, the three 1995 distributions and also all the nine distributions together. We checked the quality of the fits by including also the anchoring systematic errors, discussed in the previous section. They all have been conservatively considered uncorrelated as a function of radius, except for the error of the fit method. Uncorrelated errors on the anchors actually produce anti-correlations between adjacent bins. These short range effects may deteriorate greatly the fit  $\chi^2$  even if producing small effects on the fitted slope. We have then built  $24 \times 24$  covariance matrices implementing these systematic errors for radial distributions binned with 1 bin equal to 1 detector pad ( $2.5 \text{ mm}$ ). We checked the fit  $\chi^2$  both before and after the

Sequence number: 5  
Author: Richard Kellogg  
Subject: Highlight  
Date: 14.4.2004 6:04:04 PM

**T**replace:

To stay away from such problems we have selected  
with:

The behavior of the anchors with depth indicate that the onset of these problems is abrupt, and a large region of the detector remains well understood for use in our analysis. We have therefore selected

---

Sequence number: 6  
Author: Richard Kellogg  
Subject: Highlight  
Date: 14.4.2004 6:27:31 PM

**T**replace:

may no longer be  
with:

is evidently no longer

---

Sequence number: 7  
Author: Richard Kellogg  
Subject: Highlight  
Date: 14.4.2004 6:04:42 PM

**T**replace:

game

with:

analysis

---